www.czasopisma.pan.pl PAN www.journals.pan.pl
Metrol. Meas. Syst., Vol. 27 (2020) No. 1, pp. 51–64
DOI: 10.24425/mms.2020.131723

PAN POLSKA AKADEMIA NAUK

METROLOGY AND MEASUREMENT SYSTEMS
Index 330930, ISSN 0860-8229
www.metrology.pg.gda.pl

M&MS

AN IMPROVED CORDIC FOR DIGITAL SUBDIVISION OF MOIRÉ SIGNAL

Weibin Zhu[1)], Shengjin Ye[1)], Yao Huang[2)], Zi Xue[2)]

1) *China Jiliang University, School of Measurement and Testing Engineering, Hangzhou, 310018, China* (✉ *zhuweibn@cjlu.edu.cn,* +86 135 8806 8692)
2) *National Institute of Metrology, Beijing, 100029, China* (*huangyao@nim.ac.cn*)

Abstract

The contradiction between the restriction of grating manufacturing technology and high-resolution measurement requirements has been the focus of attention. The precision requirement of angle calculation during the digital subdivision processing of a Moiré signal is focused on, the causes of errors in the solution of arcsine function are analysed, and an improved *coordinate rotation digital computer* (CORDIC) with double-rotation iteration is proposed by discussing the principle of the conventional CORDIC in detail herein. Because the iterative number and data width of the improved CORDIC are limited by the finite digital circuit resources and thus determine the calculation accuracy directly, subsequently the *overall quantization error* (OQE) of the improved CORDIC is analysed. The approximate error and rounding error of the algorithm are deduced, and the error models of iterative number and data width are established. The validity and application value of the improved CORDIC are proved through simulations and experiments involving a subdividing circuit. The corresponding relation between the approximate error, rounding error and iteration number, as well as the bit width are proved by quantization. The error of subdivision with the improved CORDIC, obtained through a calibration experiment, is within ±0.5″ and the mean variance is 0.2″. The results of the research can be applied directly to a digital subdivision system to guide the parameter setting in the iterative process, which is of crucial importance in the quantitative analysis of error separation and error synthesis.

Keywords: grating, digital subdivision, coordinate rotation digital computer, double-rotation, overall quantization error.

1. Introduction

Grating is a typical linear displacement measurement sensor. The method consists in measurement of linear displacement or rotation angle by the Moiré fringes formed by the relative displacement between the main grating and the indicating grating. Grating presents significant advantages of large scale and high resolution and has been widely used in various scientific and industrial fields, such as incremental and absolute angular encoders, coordinate measuring machines, angle-measuring standards, robots, CNC machines *etc.* [1–4].

The measurement resolution of grating is determined by the size of grating pitch. Because of the contradiction between the restriction of grating manufacturing technology and high-resolution measurement requirements, the subdivision of a Moiré signal has become the focus of attention in the grating application field. The subdivision methods of Moiré signals can be roughly classified into two categories: based on the phase and based on the amplitude. The phase-based subdivision methods mainly include phase-locked frequency multiplier method, carrier modulation method, wavelet subdivision method *etc.* [5–7] while amongst the amplitude-based subdivision methods there are quadruple frequency subdivision, resistance chain subdivision, triangle wave subdivision and tangent subdivision methods [8–10]. From the perspective of ease of application, the latter category is more flexible and therefore it is widely used.

In practice, the digital subdivision method, in which digital circuits are employed in the amplitude-based subdivision method, have been widely used in subdivision systems because of its simple mechanism, flexibility of parameter adjustment, and convenience of high integration [11, 12]. The digital subdivision is accomplished based on the relationship between the measured position and phase of a periodic signal. The accuracy and speed of phase angle calculation are of crucial importance for digital subdivision [13, 14].

The *coordinate rotation digital computer* (CORDIC) algorithm, proposed by Jack E. Volder in 1959 [15] and unified by Walther in 1971 [16], has been widely used in digital circuits for angle calculation because of its obvious advantages of simple operation and great speed. The conventional CORDIC can solve such functions as sine, cosine, tangent, arctangent, natural logarithm, and square root. Meanwhile, a large calculation error exists with arcsine and arccosine because of the excessive convergence rate of iteration and the inevitable misjudgement of rotation direction [17].

Focusing on the calculation accuracy of CORDIC, Hu [18] proposed an error evaluation model of the conventional CORDIC and quantified the error values of sine-cosine and arctangent functions effectively but did not analyse the effectiveness and quantization error of the conventional CORDIC in calculating the arcsine function. Xie [19] proposed a piecewise correction formula to improve the calculation accuracy of the conventional CORDIC, but the introduced division operation of correction formula is a serious constraint on the implementation of an algorithmic circuit. Rajkumar [20] proposed a CORDIC error detection scheme for fixed rotation angles that effectively evaluated noise. Mazenc [21] and Liu [22] improved the iterative structure of the conventional CORDIC and calculated arcsine and arccosine functions by appropriate compensation of the modulus correction factor. In the calculation, iteration required more resources, and resource volume and quantitative error were not analysed.

In this study, we analyse the requirements of angle calculation accuracy in the digital subdivision of a grating Moiré signal; further, based on the conventional CORDIC, we propose an improved CORDIC with a double-rotation iterative structure used for the solving of arcsine function. An *overall quantization error* (OQE) model was established to analyse the factors influencing errors. The validity of the OQE model is verified by simulation and experiment and the error of subdivision with the improved CORDIC is proved by a calibration experiment. The improved CORDIC proposed herein can be used directly to calculate the phase of grating signal, and the OQE model can be used to guide the parameter setting in the iterative process.

2. Conventional CORDIC algorithm

2.1. Digital subdivision of grating Moiré signal

The output of a grating sensor is a sine-cosine Moiré signal. The displacement of each grating pitch corresponds to the period of a sine-cosine signal and the position in one grating pitch

Metrol. Meas. Syst., Vol. 27 (2020), No. 1, pp. 51–64
DOI: 10.24425/amms.2020.131723

corresponds to the phase, φ, of the sine-cosine signal. If the periodic subdivision number in one grating pitch is M, the subdivision number of current position, m, is:

$$m = \text{int}\left(\frac{\varphi}{360} \cdot M\right). \tag{1}$$

An ADC is used to sample the amplitude of the output signal of grating in the digital subdivision system. The converted amplitude digital signal is calculated by the CORDIC algorithm to obtain φ corresponding to the current measurement position. Subsequently, m is obtained by (1). The digital subdivision flowchart is shown in Fig. 1.

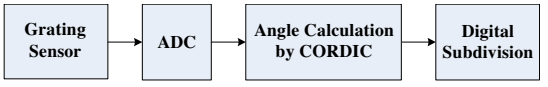

Fig. 1. A schematic of the digital subdivision flowchart.

According to Fig. 1 and (1), the angular calculation accuracy using the CORDIC algorithm will directly affect the output accuracy of the digital subdivision system. Angle calculation by CORDIC is the most basic and critical part of the digital subdivision system.

2.2. Principle of CORDIC

The angle calculation by the conventional CORDIC consists in approximating the target process through a series of Givens rotations. In the Cartesian coordinate system, the vector $(x,\ y)$ to be solved by the unit circle is as follows:

$$\begin{cases} x = \cos\theta \\ y = \sin\theta \end{cases}. \tag{2}$$

The solution is obtaining the position of $(x,\ y)$ on the unit circle. After the initial vector, $v(0)$, is rotated i times, the final vector, $v(i)$, and the target vector, $(x,\ y)$, coincide approximately. The rotation approximation process is shown in Fig. 2.

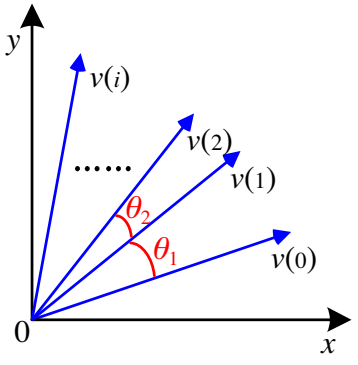

Fig. 2. A schematic diagram of the principle of CORDIC.

For the Givens rotation, the Cartesian coordinates of the vector before and after rotation can be expressed as:

$$\begin{bmatrix} x_i \\ y_i \end{bmatrix} = \begin{bmatrix} \cos\theta_{i-1} & -\sin\theta_{i-1} \\ \sin\theta_{i-1} & \cos\theta_{i-1} \end{bmatrix} \begin{bmatrix} x_{i-1} \\ y_{i-1} \end{bmatrix}. \tag{3}$$

For the convenience of digital circuit implementation, (3) is converted to:

$$\begin{bmatrix} x_i \\ y_i \end{bmatrix} = \cos\theta_{i-1} \begin{bmatrix} 1 & -\tan\theta_{i-1} \\ \tan\theta_{i-1} & 1 \end{bmatrix} \begin{bmatrix} x_{i-1} \\ y_{i-1} \end{bmatrix}. \tag{4}$$

In the conventional CORDIC algorithm, the angle of each rotation is defined as:

$$\theta_i = \arctan 2^{-i}. \tag{5}$$

Because the rotation angles of the conventional CORDIC are quantified to a series of unequal, constant angles, the angle calculation process by the conventional CORDIC is an approach using fixed values. Each rotation causes a change in the vector module length. The extension factor, K_i, is definedas:

$$K_i = \frac{1}{\cos\theta_i}. \tag{6}$$

The rotation direction identifier is defined as d_i, $d_i = -1$ when the coordinates rotate clockwise, while $d_i = +1$ when the coordinates rotate counter-clockwise. The i-th rotation can be expressed as:

$$\begin{bmatrix} x_i \\ y_i \end{bmatrix} = \begin{bmatrix} 1 & -d_i 2^{-i} \\ d_i 2^{-i} & 1 \end{bmatrix} \begin{bmatrix} x_{i-1} \\ y_{i-1} \end{bmatrix}. \tag{7}$$

2.3. Solving arcsine function by CORDIC

To solve the arcsine function for the digital subdivision, an appropriate starting position and rotation direction judgment must be set in each iteration process. The calculation process is described as:

$$\begin{cases} x_0 = 1/\prod_{i=1}^{n} K_i \\ y_0 = 0 \\ z_0 = 0 \\ d_i = \operatorname{sign}(Amp_i - y_i) \end{cases}, \tag{8}$$

Amp is an amplitude of the Moiré signal sampled by the ADC in the grating subdivision system. The direction of the next rotation is obtained by continuous comparing with the y coordinate. After execution of the iteration process n times, the orientation vector, $(x,\ y)$, can be approximated with a small error; thus, the angle value of arcsine, θ, can be obtained by z_n. Fig. 3 shows the calculation error of arcsine function calculated by the conventional CORDIC, obtained using MATLAB when $n = 15$. The calculation error is defined as the difference between the arcsine angle value calculated by CORDIC algorithm and the theoretical phase value for a given sine.

As shown in Fig. 3, the conventional CORDIC exhibits a large calculation error in some angle intervals. The primary reason is that in the iterative process the vector modulus length increases gradually because of the extension factor K_i, while the target vector modulus length is fixed. This rotation iteration method causes a misjudgement of the rotation direction and results in a larger calculation error.

www.czasopisma.pan.pl PAN POLSKA AKADEMIA NAUK
Metrol. Meas. Syst., Vol. 27 (2020), No. 1, pp. 51–64
DOI: 10.24425/amms.2020.131723

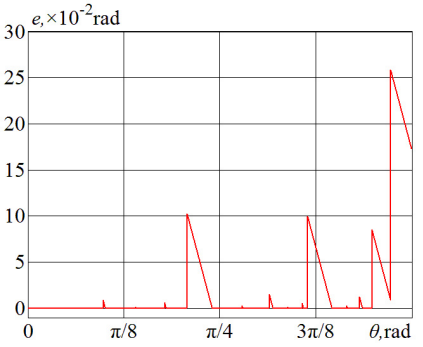

Fig. 3. A calculation error curve of the conventional CORDIC.

3. Improved CORDIC algorithm

When the arcsine function is resolved by the conventional CORDIC, it is impossible to calculate the extension factor accurately, thus causing an error in angle calculation.

In the improved CORDIC algorithm, two rotation steps exist with the same angle in each iterative process, called the double-rotation method. The rotation process is shown in Fig. 4.

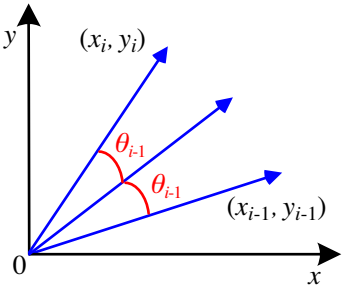

Fig. 4. A schematic diagram of the double-rotation process.

The double-rotation process is expressed as follows:

$$\begin{bmatrix} x_i \\ y_i \end{bmatrix} = \begin{bmatrix} \cos 2\theta_{i-1} & -\sin 2\theta_{i-1} \\ \sin 2\theta_{i-1} & \cos 2\theta_{i-1} \end{bmatrix} \begin{bmatrix} x_{i-1} \\ y_{i-1} \end{bmatrix}. \tag{9}$$

With the equivalent transformation of a trigonometric function, (9) is converted to:

$$\begin{bmatrix} x_i \\ y_i \end{bmatrix} = \begin{bmatrix} 1-\tan^2\theta_{i-1} & -2\tan\theta_{i-1} \\ 2\tan\theta_{i-1} & 1-\tan^2\theta_{i-1} \end{bmatrix} \begin{bmatrix} x_{i-1} \\ y_{i-1} \end{bmatrix}. \tag{10}$$

The extension factor in the double-rotation method, K_{D_i}, is defined as:

$$K_{D_i} = 1/\cos^2\theta_i\,. \tag{11}$$

The formula for K_{D_i} is transformed to:

$$K_{D_i} = \frac{1}{\cos^2\theta_i} = 1 + 2^{-2i}. \tag{12}$$

Formula (12) shows that K_{D_i} can be calculated using only shift and add operations, which is extremely convenient in implementing it in digital circuits.

The formulae for calculating the angle of arcsine function with the improved CORDIC are the following:

$$\begin{cases} x_1 = 0, \quad y_1 = Amp_1, \quad z_1 = \pi/2 \\ d_i = \text{sign}(y_i - Amp_i), \quad z_i > \pi/2 \\ x_{i+1} = (1 - 2^{-2i})x_i + d_i \cdot 2^{1-i} \cdot y_i \\ y_{i+1} = (1 - 2^{-2i})y_i - d_i \cdot 2^{1-i} \cdot x_i \\ z_{i+1} = z_i - d_i \cdot 2\theta \\ Amp_{i+1} = Amp_i \cdot K_i \end{cases} . \tag{13}$$

The rotation angle is $2\theta_i$ in each iterative process and K_{D_i}, calculated accurately with (12), is introduced simultaneously to compensate the change in modulus length caused by rotation. Namely, *Amp* is amplified with the value of K_{D_i}. The computation process can be executed by only shift and add operations, which is convenient for implementation in hardware.

Using (13), the modulus length of the vector to be solved is invariable during rotation and the problem of direction misjudgement is avoided. Fig. 5 shows the calculation error of arcsine function calculated by the improved CORDIC, obtained using MATLAB when $n = 15$.

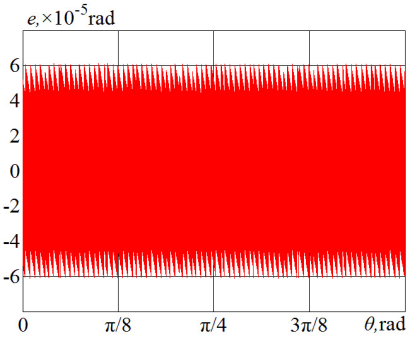

Fig. 5. A calculation error curve for the improved CORDIC.

The error of the improved CORDIC algorithm is within $\pm 6 \times 10^{-5}$ rad, which is much smaller than that shown in Fig. 3.

4. OQE analysis

In the digital subdivision system of a grating Moiré signal, the improved CORDIC algorithm is implemented in a digital circuit. The iterative number, n, and data width, b, of the CORDIC are limited by the finite digital circuit resources and thus determine the calculation accuracy directly. Therefore, it is particularly important to choose suitable n and b according to the precision requirement of the digital subdivision system.

Two error sources are involved in the improved CORDIC algorithm. One error, called the approximate error, is caused by using finite times of rotation approximation value as the calculation result, the other, called the rounding error, is caused by a finite data width limited by the digital circuit.

4.1. Approximation error

Using the improved CORDIC algorithm to resolve the angle, the rotation angle value of each iterative process is:

$$a_i = 2\theta_i = 2 * \arctan(2^{-i}). \tag{14}$$

After n iterations, the angle value, A, is obtained by accumulation of the rotation angle. At this time, the approximate error is assumed to be δ, and A is expressed as:

$$A = \theta_1 + \sum_{i=1}^{n} d_i * a_i + \delta, \tag{15}$$

where θ_1 is the initial angle.

The vector after n rotations, $(x_{n+1},\ y_{n+1})$, is located in an interval $[A - |\delta|,\ A + |\delta|]$. Because the target vector location is random, the approximation error obeys a uniform distribution. The approximation error value affects the solving accuracy of arcsine function directly. The maximum approximation error, $\delta_{\max}$, is expressed as:

$$\delta_{\max} = 2 \cdot \arctan 2^{-n} < 2^{1-n}. \tag{16}$$

When the value of iterative number is sufficiently large, (16) is transformed to:

$$\delta_{\max} = \lim_{n \to +\infty} 2 \cdot \arctan 2^{-n} = 0. \tag{17}$$

Formula (17) shows that increasing n can reduce the approximation error. The larger the iterative number, the smaller the approximation error.

4.2. Rounding error

The rounding error of z_i in the iterative process is only related to the calculation accuracy of the angle, which can be determined directly according to the maximum permissible errors of the angle. If $e(i) \equiv [e_x(i),\ e_y(i)]$ is the rounding error vector after the i-th iteration, the absolute rounding error of x and y will be bounded by:

$$\begin{cases} |e_x(i)| \le \varepsilon \\ |e_y(i)| \le \varepsilon \end{cases}. \tag{18}$$

The magnitude of rounding error, ε, is determined by the bit width of binary digits of the internal registers in the calculation process. If the fixed point representation has "b" binary digits while the sign bit is not taken into account, the rounding error is:

$$\varepsilon = 2^{-b-1}. \tag{19}$$

Therefore, the upper bound of $|e(i)|$ is:

$$|e(i)| \equiv \sqrt{e_x^2(i) + e_y^2(i)} \le \sqrt{2}\varepsilon. \tag{20}$$

For the i-th double-rotation process, the transformed matrix of modulus is:

$$P(i) = K_{D_i} \cdot \begin{bmatrix} \cos[d_i \cdot a_i] & -\sin[d_i \cdot a_i] \\ \sin[d_i \cdot a_i] & \cos[d_i \cdot a_i] \end{bmatrix}. \tag{21}$$

The rounding error is introduced from two sources. One is the rounding error of the current iteration and the other is the accumulated error before the current iteration. Set $\hat{v}(i)$ as the iteration vector before rounding off the i-th iteration and $v(i)$ as the iteration vector after rounding off. Thus,

$$\hat{v}(i) = v(i) + e(i). \tag{22}$$

Define $Q[*]$ to be the cumulative error propagation operator; subsequently, $P(i)\,Q[v(i)]$ is the rounding error before the current iteration. Namely:

$$Q\left[\hat{v}(i+1)\right] = P(i)Q\left[\hat{v}(i)\right] + e(i+1). \tag{23}$$

Define $f(n)$ to be the total rounding error of $v(n+1)$ after n iterations:

$$f(n) = Q\left[\hat{v}(n+1)\right] - v(n+1) = e(n) + \sum_{j=1}^{n}\left\{\prod_{i=j}^{n} P(i)e(i)\right\}. \tag{24}$$

Based on the above formula, we obtain:

$$\begin{cases} |f(n)| <= 2^{-b-0.5}\cdot G(n) \\ G(n) = 1 + \sum\limits_{j=1}^{n}\prod\limits_{i=j}^{n}\|P(i)\| = 1 + \sum\limits_{j=1}^{n}\prod\limits_{i=j}^{n}(1+2^{-2i}) \end{cases}. \tag{25}$$

According to (25), after n iterations the target vector is $v(n+1) = [x(n+1),\ y(n+1)]^T$ and Amp is amplified by the same extension factor; namely, the rounding error of $y(n+1)$ and Amp are:

$$\begin{cases} \varepsilon_y = |f(n)| = 2^{-b-0.5}\cdot G(n)\cdot\sin\theta \\ \varepsilon_{Amp} < 2^{-b-0.5}\cdot G(n) \end{cases}. \tag{26}$$

4.3. OQE model

Because of the rounding error of $y(n+1)$ after iteration, the solved value of arcsine function is smaller than the target angle. Because the maximum deviation exists near $\pi/2$, the maximum absolute rounding error of solving arcsine function, $\varepsilon_{\max}$, can be evaluated as:

$$\varepsilon_{\max} = \left|\arcsin(\sin\theta - \varepsilon_y) - \theta\right| \le \pi/2 - \arcsin(1 - 2^{-b-0.5}\cdot G(n)). \tag{27}$$

Combining the approximation and rounding errors, the overall quantization error of solving arcsine function with the double-rotation method, Δ_{OQE}, is:

$$\Delta_{\mathrm{OQE}} = \delta_{\max} + \varepsilon_{\max} \le 2^{1-n} - \arcsin\left(1 - 2^{-b-0.5}\cdot G(n)\right) + \pi/2. \tag{28}$$

As shown in (28), the magnitude of Δ_{OQE} depends on n and b. For given n and b values, the error of the improved CORDIC algorithm can be evaluated conveniently.

5. Experiment and analysis

The effectiveness of the improved CORDIC algorithm has been demonstrated by comparing Fig. 3 with Fig. 5. Further, the OQE values have been verified experimentally and applied to the digital subdivision system.

Metrol. Meas. Syst., Vol. 27 (2020), No. 1, pp. 51–64
DOI: 10.24425/amms.2020.131723

5.1. Simulation experiments of approximate error and rounding error

The approximate error, δ, is only related to the iteration order, n. The simulation results of the relationship between $\delta_{\max}$ and n aided by MATLAB are shown in Fig. 6.

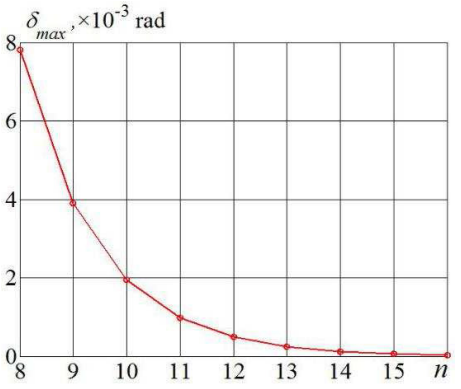

Fig. 6. The relationship between $\delta_{\max}$ and n.

As shown in Fig. 6, with an increase of n, $\delta_{\max}$ converges rapidly. The value of $\delta_{\max}$decreases by approximately half for every increment of n by 1 and the simulation result is in agreement with (17).

The rounding error, $\varepsilon_{\max}$, affected by n and b, will decrease as b increases according to (27). The simulation results, aided by MATLAB, of the relationship between $\varepsilon_{\max}$, n and b for $n = 12-16$ and $b = 16-32$ are shown in Fig. 7.

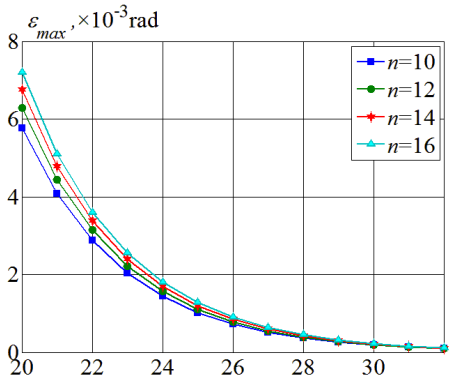

Fig. 7. The relationship between $\varepsilon_{\max}$ and b.

As shown in Fig. 7, the rounding error converges rapidly with an increase in b and the attenuation curve trend is the same for different values of n. When b is increased to a certain extent, the rounding error of different iterations is approximately equal.

The values of n and b can be determined according to the simulation results. In hardware implementation as well as in software design, the minimum values of n and b to satisfy the precision requirement of the subdivision can be selected conveniently. There can be considered both hardware resource occupation and subdivision accuracy.

5.2. Circuit experiments of OQE

To verify the effectiveness of the improved CORDIC in solving arcsine function, the simulation values and circuit experimental results are compared and analysed in this section.

According to (28), the simulation values of OQE, defined as Δ_{OQEs}, for $n = 13, 14, 15$ and $b = 26, 28, 30, 32$, are simulated and shown in Table 1.

Table 1. Values of ΔOQEs and ΔOQEp ($\times 10^{-4}$ rad).

	$n = 13$		$n = 14$		$n = 15$	
	ΔOQEs	**ΔOQEp**	**ΔOQEs**	**ΔOQEp**	**ΔOQEs**	**ΔOQEp**
$b = 26$	6.80733	3.12919	5.82284	1.90849	5.43715	1.29813
$b = 28$	4.62437	2.45193	3.52177	1.40353	3.02375	1.14327
$b = 30$	3.53289	2.44758	2.37124	1.22688	1.81705	0.94804
$b = 32$	2.98715	2.43569	1.79597	1.21499	1.21370	0.61007

Circuit experiments were performed using a homemade electronic board, as shown in Fig. 8. The arcsine function was solved with the improved CORDIC, and the grating signal was subdivided in an FPGA chip.

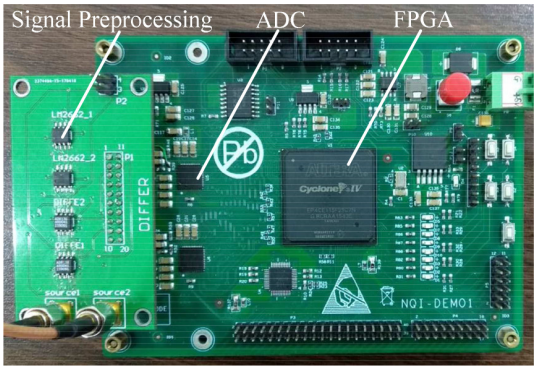

Fig. 8. The experimental homemade electronic board.

Affected by such factors as grating adjustment error, photoelectric device position offset, photosensitive element nonlinearity and environment temperature, the Moiré signals usually have unequal amplitude, DC drift, non-orthogonality and harmonic components. Focusing on the effect of CORDIC algorithm on subdivision, the above noise should be abandoned, so that a signal generator (RIGOL DG4162) was selected as the signal source to simulate a sinusoidal signal with a frequency of 10 K. In the homemade electronic board, there are used a 16-bit ADC and a sampling rate 40 MSa/s. An EP4CE115F29C7 chip of Altera Company was employed as the FPGA.

Setting the same values of n and b as the simulation values, namely $n = 13, 14, 15$ and $b = 26, 28, 30, 32$, the angle values of arcsine function were solved with the circuit, while the theoretical angle values were calculated in MATLAB using the sampling amplitude of the input signal of the circuit. During the calculation process by the circuit and MATLAB, n and b are both represented as fixed point, signed numbers. The maximum difference of two angle values used as the circuit experiment values of OQE, defined as Δ_{OQEp}, is shown in Table 1.

Metrol. Meas. Syst., Vol. 27 (2020), No. 1, pp. 51–64
DOI: 10.24425/amms.2020.131723

As shown in Table 1:

1. Because (28) is the maximum error model and Δ_{OQEs} is the value when each error reaches the maximum simultaneously, $\Delta_{OQEs} > \Delta_{\mathrm{OQEp}}$ always exists for different n and b values.
2. For different b values, both Δ_{OQEs} and Δ_{OQEp} will decrease gradually when the n value is changed from small to large. The change trend coincides with the curve of Fig. 6.
3. For different n values, both Δ_{OQEs} and Δ_{OQEp} will decrease gradually when changing the b value from small to large. The change trend coincides with the curve of Fig. 7.

5.3. Grating digital subdivision experiment

We verified the effect of the improved CORDIC algorithm in the grating digital subdivision circuit. We set $M = 256, 512, 1024$, and used the conventional CORDIC and improved CORDIC separately in the digital subdivision circuit. The subdivision of the achieved results for three different values of n and b is shown in Table 2.

Table 2. Completion of subdivision with conventional CORDIC and improved CORDIC.

M	(n, b)	Conventional CORDIC	Improved CORDIC
256	(8, 16)	not achieved	achieved
	(9, 18)	not achieved	achieved
	(10, 20)	not achieved	achieved
512	(8, 16)	not achieved	not achieved
	(9, 18)	not achieved	achieved
	(10, 20)	not achieved	achieved
1024	(8, 16)	not achieved	not achieved
	(9, 18)	not achieved	not achieved
	(10, 20)	not achieved	achieved

As shown in Table 2:

1. Owing to the principle error, the conventional CORDIC cannot easily satisfy the accuracy requirements of the digital subdivision. Even for the conditions of $n = 10$ and $b = 20$, $M = 256$ still cannot be achieved. Instead, the implementation results of the improved CORDIC algorithm are much better.
2. With the improved CORDIC algorithm, $M = 256$ can be achieved in all three operating conditions. As the periodic subdivision number, M, becomes larger, the accuracy requirements of the digital subdivision become higher. It is difficult to ensure the subdividing function of higher M for smaller values of $(n,\ b)$. The values of $(n,\ b)$ must be increased to satisfy the requirement of higher precision.

5.4. Calibration experiment of grating digital subdivision

In order to quantify the subdivision error of the subdivision method with the improved CORDIC, an experimental calibration system was constructed, as shown in Fig. 9.

The grating code disk is installed on the bearing platform through a coupling while grating reading head is installed on the reading head stand. The position of the laser interferometer is adjusted by the lift table, so that it is located at the same horizontal line with the angle interferoscope and angle reflector.

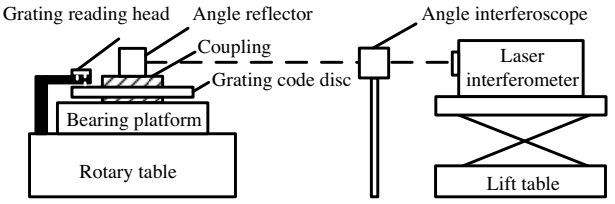

Fig. 9. A schematic of the experimental calibration device.

While the rotary table rotates, the reading head outputs Moiré signals. Then the signals are subdivided 1024 times with the homemade electronic board with the improved CORDIC. Furthermore, the measurement results are calibrated by a Renishaw XL-80 laser interferometer. The real experiment setup is shown in Fig. 10 and the specifications of the main instruments used in the experiments are shown in Table 3.

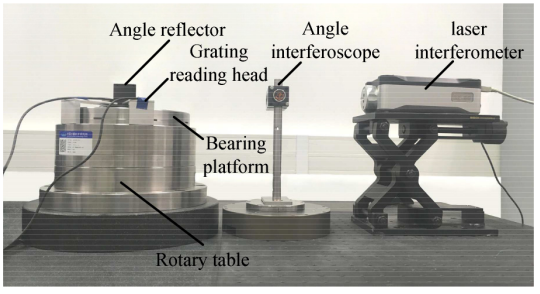

Fig. 10. The experiment setup.

Table 3. Specifications of the main instruments.

Instrument	Model (manufacturer)	Specification
The laser Interferometer angle standard	XL-80/150 mm (RENISHAW)	Measuring range: From -1° to $+1^\circ$ $U_i = 0.05''$ ($k = 2$)
Rotary glass scales	R10851 (MicroE system)	16384 CPR grating pitch: 20 μm
Reading Head	Mercury's sensor (MicroE system)	Rotary: Up to ±2.1″ (arc sec)

In a range of 160″ (a little bigger than 2 grating pitch), we have obtained test data with a 0.2″ displacement in each step. The angle measurement results of the laser interferometer and homemade electronic board are synchronously obtained with the improved CORDIC and the calibration errors, defined as the difference between two measurement results of angular displacement, are shown in Fig. 11.

As shown in Fig. 11, the calibration error can be within ±0.5″ and the mean variance is 0.2″. Here, the angular resolution of the grating grid is 79.1″, and the relative calibration error is ±0.632%. Limited to the stability of optical systems and turntable structures, there is still some deviation from the theoretical subdivision results. The difference between them may be caused by the cumulative errors of the grating period and a slight misalignment between the reading head and the scale grating.

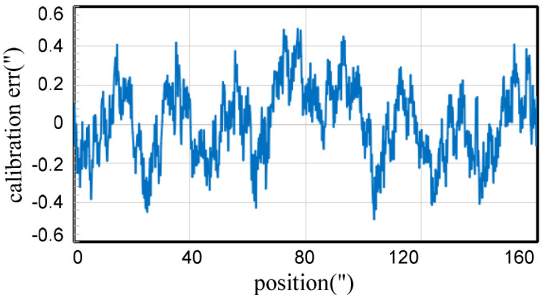

Fig. 11. Experiment results of calibration error.

6. Conclusions

In accordance with the accuracy requirement in the digital subdivision of the grating signal, we first studied the principle of the conventional CORDIC herein. By analysing the problem where the principle error of the conventional algorithm is extremely large in solving arcsine signal, an improved CORDIC with double-rotation iteration was proposed and the principle error of the angle solution was reduced. Next, the OQE of the improved CORDIC was analysed and the approximate error and rounding error of the improved algorithm were deduced; subsequently, the error models of the iterative number and data width were established. Finally, simulations and circuit experiments were performed to verify the improved CORDIC, the rationality of overall quantization error, and the application value in the actual grating signal digital subdivision. The results of the research can be applied directly to the grating digital subdivision system, which is crucial to the quantitative analysis of error separation and error synthesis.

Acknowledgements

This research was financially supported by the project of the National Key R&D Program of China (2017YFF0204901), the research project of General Administration of Quality Supervision, Inspection and Quarantine of PRC (2016QK189).

References

[1] Huang, Y., Xue, Z., Huang, M., Qiao, D. (2018). The NIM continuous full circle angle standard. *Measurement Science and Technology*, 29(7).

[2] Huang, Y., Xue, Z., Qiao, D., Wang, Y. (2017). Study on the metrological performance of self-calibration angle encoder. *Proc. SPIE 9684*.

[3] Wataru, K., Tsukasa, W., Hideaki, N., Akihiro, O. (2017). Angular velocity calibration system with a self-calibratable rotary encoder. *Measurement*, 82(1), 246–253.

[4] Just, A., Krausea, M., Probsta, R., Bossea, H., Haunerdingerb, H., Spaethb, Ch., Metzb, G., Israel, W. (2009). Comparison of angle standards with the aid of a high-resolution angle encoder. *Precision Engineering*, 33(2), 530–533.

[5] Emura, T., Wang, L. (2000). A high-resolution interpolator for incremental encoders based on the quadrature PLL method. *IEEE Transactions on Industrial Electronics*, 47(1), 84–90.

[6] Chang, L., Xu, H., Zhou, Y., Zhang, J. (2009). All Digital Phase Detection and Tracking Method to Subdivide the Grating Moiré Fringe Signal. *International Asia Conference on Informatics in Control, Automation and Robotics*, Bangkok, 469–472.

[7] Angrisani, L., Capriglione, D., Cerro, G., Ferrigno, L., Miele, G. (2017). Analysis of different wavelet segmentation methods for frequency-domain energy detection based spectrum sensing. *IEEE International Instrumentation and Measurement Technology Conference (I2MTC)*, Turin, 1–6.

[8] Feng, Yingqiao, *et al.* (2013). Interpolation Error Correction of Moiré Fringe Photoelectric Signals in the Approximate Form of Triangle Wave. *Acta Optica Sinica*, 33(8), 106–110.

[9] Liu, B., Li, J. (2011). Research on signal subdivision of grating sensor. *Proc. of 2011 6th International Forum on Strategic Technology*, Harbin, Heilongjiang, 1235–1238.

[10] Lv, M., Guo, Q., Zhang, C. (2010). Noise filtering for Moire Fringe signals based on variable step size adaptive neural network algorithm. *Proc. of SPIE – The International Society for Optical Engineering*, 7656(19), 76567L–76567L-7.

[11] Angrisani, L., Capriglione, D., Cerro, G., Ferrigno, L., Miele, G. (2017). Analysis of different wavelet segmentation methods for frequency-domain energy detection based spectrum sensing. *IEEE International Instrumentation and Measurement Technology Conference*.

[12] Dragan, Ž., Milan, S., Zivko, K., Dragan, D., Vladimir, D. (2018). Generation of Long-time Complex Signals for Testing the Instruments for Detection of Voltage Quality Disturbances. *Measurement Science Review*, 18(2), 41–51.

[13] Emura, T., Wang, L. (2000). A high-resolution interpolator for incremental encoders based on the quadrature PLL method. *IEEE Transactions on Industrial Electronics*, 47(1), 84–90.

[14] Jelena, J., Dragan, Uglješa, J. (2018). An Improved Linearization Circuit used for Optical Rotary Encoders. *Measurement Science Review*, 17(5), 241–249.

[15] Volder, J.E. (1959). The CORDIC trigonometric computing technique. *IRE Transactions on Electronic Computers*, 8(3), 330–334.

[16] Walther, J.S. (1971). A unified algorithm for elementary functions. *Spring Joint Computer Conf.*, 18(20), 379–385.

[17] Aggarwal, S., Meher, P.K. (2016). Concept, Design, and Implementation of Reconfigurable CORDIC. *IEEE Transactions on Very Large Scale Integration (VLSI) Systems*, 24(4), 1588–1592.

[18] Hu, Y.H. (1992). The quantization effects of the CORDIC algorithm. *IEEE Transations on Signal Proc.*, 40(4), 834–844.

[19] Shanying, X., Weiming, Q., Xiaoning, C. (2010). Implement of Arcsine Function Based on FPGA. *Chinese Journal of Electron Devices*, 33(3), 344–347.

[20] Rajkumar, R. (2016). Reliable Hardware Architectures of the CORDIC Algorithm With a Fixed Angle of Rotations. *IEEE Circuits and Systems Society*, 64(8), 972–976.

[21] Mazenc, C., Merrheim, X., Muller, J.M. (1993). Computing functions arccos and arcsin using CORDIC. *IEEE Transactions on Computers*, 42(1), 118–122.

[22] Liu, X., Xie, Y., Chen, H. (2015). Implementation on FPGA for CORDIC-based Computation of Arcsine and Arccosine. *IET International Radar Conference 2015*.